



# Effect of sol-layers on Sb-doped SnO<sub>2</sub> thin films as solution-based transparent conductive oxides

Ha-Rim An<sup>a</sup>, ChangYeoul Kim<sup>b</sup>, Sung-Tag Oh<sup>a</sup>, Hyo-Jin Ahn<sup>a,\*</sup>

<sup>a</sup>Department of Materials Science & Engineering, Seoul National University of Science and Technology, Seoul 139-743, Republic of Korea

<sup>b</sup>Future Convergence Ceramic Division, Korea Institute Ceramic Engineering and Technology (KICET), Seoul 233-5, South Korea

Received 21 May 2013; received in revised form 4 June 2013; accepted 4 June 2013

Available online 18 June 2013

## Abstract

We synthesized dense Sb-doped SnO<sub>2</sub> (ATO) thin films coated with the optimum number of sol-layers to form solution-based transparent conductive oxides (TCOs) using a hydrothermal method and spin-coating. To investigate the effects of the sol-layers on the ATO thin films, samples with 0, 1, 3, 5, and 7 sol-layers were deposited on ATO thin films with porous surface morphologies. The structures, chemical states, morphology changes, and electrical and optical properties of the samples were demonstrated using X-ray diffraction (XRD), X-ray photoelectron spectroscopy (XPS), field-emission scanning electron microscopy (FESEM), atomic force microscopy (AFM), transmission electron microscopy (TEM), Hall effect measurement, and UV–vis spectrophotometry. In particular, ATO thin films coated with 5 sol-layers exhibit superb resistivity, good transmittance, and a superb figure of merit (FOM) compared to the other samples. The performance enhancement could be explained in two ways; (1) densification and thickness increase by sol coating and finally, (2) the dominant increase of the carrier concentration with small decrease of the electron mobility.

© 2013 Elsevier Ltd and Techna Group S.r.l. All rights reserved.

**Keywords:** A. Films; A. Microwave processing; B. Surfaces; C. Electrical properties; C. Optical properties; Sb-doped SnO<sub>2</sub>

## 1. Introduction

Transparent conductive oxides (TCOs), which simultaneously satisfy the requirements of high electrical conductivity and high optical transparency in the visible region (~400 nm to 800 nm), have received considerable interest for applications in optoelectronic devices such as flat panel displays, touch screens, light emitting diodes, and thin film solar cells [1,2]. For these applications, TCOs must have good properties such as a wide band gap (> 3 eV), a high carrier density ( $\geq 10^{20}$  cm<sup>-3</sup>), good electrical conductivity ( $\rho \leq 10^{-3}$  Ω cm), and a high Hall mobility ( $\geq 62.5$  cm<sup>2</sup>/Vs) [3]. Among the various TCO materials (i.e., Cd, In, Sn, Zn, and Ga-based oxides), Sn-doped In<sub>2</sub>O<sub>3</sub> (ITO) is most widely used because of its various advantages including an intrinsic band gap of 3.7 eV, an electrical resistivity of  $\sim 2 \times 10^{-4}$  Ω cm, and a

transmittance of ~90% [4,5]. However, the price of indium is gradually increasing with the rapidly growing demand for ITO together with the scarcity of metal indium. Thus, many researchers are currently trying to find a substitute for ITO. Among the above-mentioned TCOs, Sb-doped SnO<sub>2</sub> (ATO) is one of the most promising candidates for replacing ITO because of its high transparency of ~80% and low resistivity of  $\sim 10^{-3}$  Ω cm as well as its good mechanical hardness and environmental stability [6]. Until now, synthetic methods carried out under vacuum conditions have mostly been developed for fabricating ATO thin films, such as sputtering, chemical vapor deposition, and electron-beam methods [7–9]. However, recent research trends are changing from vacuum-based deposition to solution-based deposition methods (i.e., spin coating, ink-jet printing, chemical baths, and dip coating) because of their ease of processing, scalability, and lower cost of device manufacturing [10]. For example, Burgard et al. fabricated ATO thin films using a spin-coating method after making a colloidal suspension of ATO powders and obtained a

\*Corresponding author. Tel.: +82 2 970 6622; fax: +82 2 973 6657.

E-mail address: [hjahn@seoultech.ac.kr](mailto:hjahn@seoultech.ac.kr) (H.-J. Ahn).

resistivity of  $3.7 \times 10^{-2} \Omega \text{ cm}$  and an optical transmittance of 90% [11]. Hwang et al. prepared ink-jet printed ITO thin films with inks composed of ITO particles and obtained an electrical resistivity of  $3 \times 10^{-2} \Omega \text{ cm}$ . To further decrease the electrical resistivity of the thin films, an Ag grid was placed between two layers of ITO films [12]. Fang et al. reported Mn-doped ZnO (MZO) thin films grown by chemical bath deposition. The electrical resistivity and transmittance of these MZO thin films were  $5.8 \times 10^{-2} \Omega \text{ cm}$  and 75.6%, respectively [13]. So far, solution-based TCOs have displayed relatively poor electrical properties because of their porous surface morphologies as thin films. To improve their electrical performance, a study on the optimum conditions for depositing sol-layers on ATO thin films with porous surface morphologies has not yet been conducted. Thus, in this study, we fabricated dense ATO thin films with various numbers of sol-layers using spin coating and demonstrated their structural, chemical, morphological, electrical, and optical properties.

## 2. Experimental

### 2.1. Experimental

In order to synthesize ATO nanoparticles using a hydrothermal method, tin (IV) chloride pentahydrate ( $\text{SnCl}_4 \cdot 5\text{H}_2\text{O}$ , Aldrich) was dissolved in an aqueous solution of  $\text{NH}_4\text{OH}$ . Then, antimony (III) chloride ( $\text{SbCl}_3$ , Aldrich) was added to the above-mentioned solution to adjust the molar ratio of Sn: Sb=10:1. After 1 h of stirring, the yellowish solution was transferred into a Teflon-lined autoclave and hydrothermal reactions were allowed to proceed at  $240^\circ\text{C}$  for 6 h. Then, the resultant precipitates were washed several times with DI water and dried in an oven at  $80^\circ\text{C}$  for 6 h. The resultant ATO nanoparticles were dispersed in ethyl alcohol (99%, DUK-SAN) with BYK 111 as a dispersant. To obtain a homogeneous solution, the mixed solution was dispersed using an ultrasonic homogenizer and a ball milling process. The prepared solution was spin-coated on the glass substrates (Corning Eagle XG) at 2000 rpm for 30 s. Then, these spin-coated glass substrates were annealed in an air atmosphere under microwave irradiation at  $550^\circ\text{C}$ . To investigate the effect of the sol-layers on the ATO films, sol solutions consisting of tin (IV) chloride pentahydrate and antimony (III) chloride dissolved in 2-propanol were spin-coated on the annealed ATO films at 2000 rpm for 30 s. Then, ATO films coated with the sol solutions were microwave-heated at  $550^\circ\text{C}$ . The number of sol layers was controlled at 0, 1, 3, 5, and 7 to determine which conditions led to the optimum performance of TCOs (referred to as 0 layer/ATO, 1 layer/ATO, 3 layer/ATO, 5 layer/ATO, and 7 layer/ATO, respectively).

### 2.2. Characterization

The structural, chemical, and morphological properties of all the samples were characterized using X-ray diffraction (XRD, Rigaku X-ray diffractometer equipped with  $\text{Cu K}\alpha$  radiation),

X-ray photoelectron spectroscopy (XPS, ESCALAB 250 equipped with an  $\text{Al K}\alpha$  X-ray source), and field-emission scanning electron microscopy (FESEM, Hitachi S-4700). The surface roughness of the ATO films was measured using atomic force microscopy (AFM, Albatross II). The structural properties of the ATO nanoparticles in thin films were measured using transmission electron microscopy (TEM, JEOL-2100F operated at 200 kV, KBSI Suncheon Center). The electrical and optical properties of the ATO films were characterized using a Hall effect measurement system (Ecopia, HMS-3000) and a UV–vis spectrophotometry (Scinco, S-3100).

## 3. Results and discussion

Fig. 1 presents XRD plots of all the samples obtained after microwave irradiation at  $550^\circ\text{C}$ . The main diffraction peaks of the samples were observed at  $26.73^\circ$ ,  $33.94^\circ$ ,  $38.07^\circ$ , and  $51.68^\circ$ , corresponding to the (110), (101), (200), and (211) planes of the tetragonal rutile structure of the cassiterite  $\text{SnO}_2$  phases (space group  $P4_2/mnm$  [136], JCPDS no. 77-0447). In particular, the diffraction peaks of the samples were slightly shifted to higher  $2\theta$  because the ionic radius of  $\text{Sb}^{5+}$  ( $0.62 \text{ \AA}$ ) is smaller than that of  $\text{Sn}^{4+}$  ( $0.69 \text{ \AA}$ ). This result is known to be derived from Bragg's law ( $n\lambda = 2d \sin \theta$ ). Furthermore, no diffraction peaks other than these main peaks was observed, which implies that all Sb ions replaced Sn ions in the  $\text{SnO}_2$  [14]. The peak intensity of the ATO films increased as the number of sol layers increased, which can be attributed to the enhanced thickness of ATO films and the enhanced crystallinity due to the larger grain size of the ATO nanoparticles [15]. Thus, polycrystalline ATO thin films with a tetragonal rutile structure were successfully synthesized.

To investigate the chemical bonding states of the samples, XPS measurements were carried out. All peak positions were adjusted using the C 1s peak at 284.5 eV. Fig. 2 shows the XPS spectra of the Sb 3d core level and Sn 3d core level obtained from the 0 layer/ATO (without sol-layers) and 5 layer/ATO films, respectively. The Sb  $3d_{5/2}$  and Sb  $3d_{3/2}$  photoelectrons of these two samples are observed at  $\sim 530.8 \text{ eV}$  and  $\sim 540.1 \text{ eV}$ , corresponding to the  $\text{Sb}_2\text{O}_5$

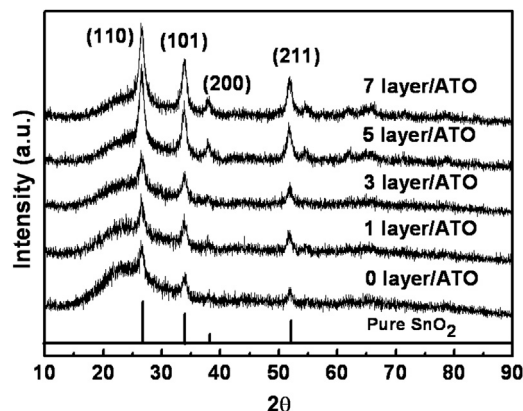


Fig. 1. XRD data obtained from 0 layer/ATO, 1 layer/ATO, 3 layer/ATO, 5 layer/ATO, and 7 layer/ATO thin films.

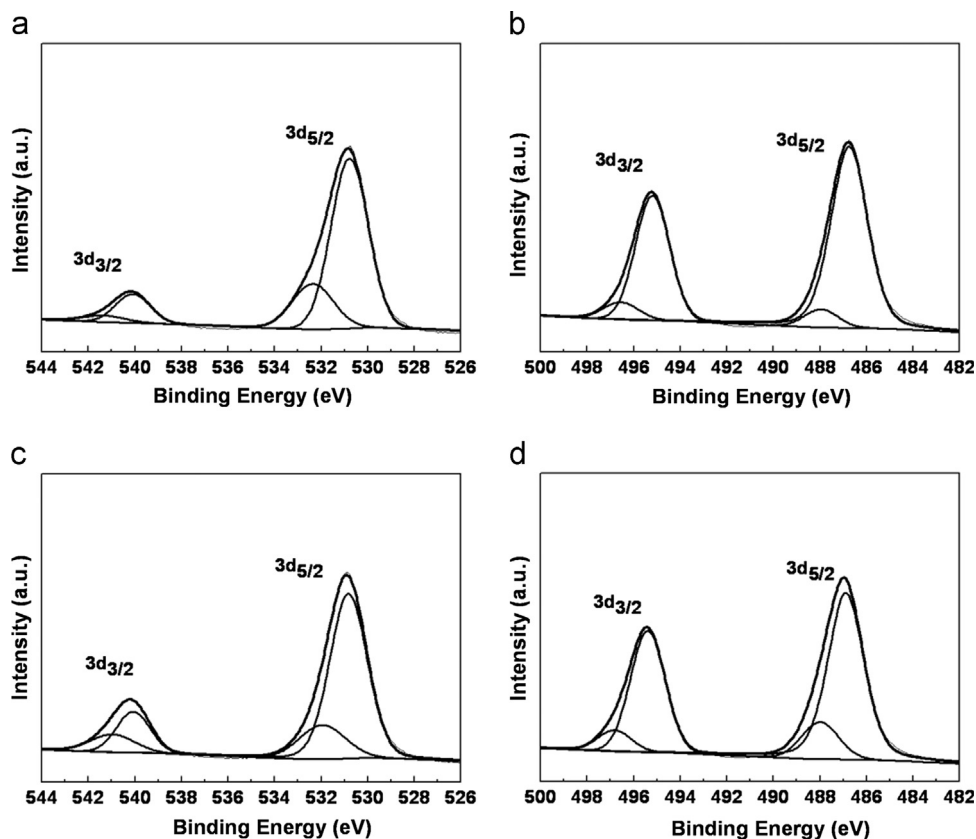


Fig. 2. XPS spectra of the Sb 3d and Sn 3d core levels for the 0 layer/ATO (a and b) and 5 layer/ATO thin films (c and d).

phases. Furthermore, the Sn  $3d_{5/2}$  and Sn  $3d_{3/2}$  photoelectrons of these two samples are observed at  $\sim 486.8$  eV and  $\sim 495.2$  eV, corresponding to the  $\text{SnO}_2$  phases [16]. This implies that the Sb and Sn phases contain the Sb (V) species and Sn (IV) species, indicating that the ATO thin films consist of  $\text{Sb}_2\text{O}_5$  and  $\text{SnO}_2$  phases. It is noted that ATO thin films were successfully formed based on the XRD and XPS results.

Fig. 3 shows top-view FESEM images of 0 layer/ATO, 1 layer/ATO, 3 layer/ATO, 5 layer/ATO, and 7 layer/ATO thin films (a–e) obtained after microwave irradiation at  $550^\circ\text{C}$ . The grain size of the 0 layer/ATO thin film ranged from  $\sim 15.0$  to  $41.2$  nm. This film exhibits a bigger inter-grain boundary between grains, implying a porous structure of the ATO thin film. TCOs with porous surface morphologies yield poor electrical properties because of the increased scattering at the grain boundaries formed in the thin films. Thus, in order to obtain dense structures of the ATO thin films, we deposited 1 (b), 3(c), 5(d), and 7(e) sol-layers on the ATO thin films. The sol-layer-coated samples have dense surface morphologies compared to the ATO thin films without sol-layers. Furthermore, it is noted that the ATO thin films coated with 7 sol-layers forms cracks, as shown in Fig. 3(e) (see arrow). In particular, possible reasons causing cracks in 7 sol-layers on the ATO thin films are increased thickness and relatively fast heating rates during annealing [17,18]. These cracks can cause a decrease in Hall mobility, resulting in a performance drop of the TCO films. Fig. 3(f–j) shows cross-sectional FESEM images of all the samples. The thicknesses of the

ATO thin films are  $\sim 290$  nm for 0 layer/ATO,  $\sim 325$  nm for 1 layer/ATO,  $\sim 381$  nm for 3 layer/ATO,  $\sim 454$  nm for 5 layer/ATO, and  $\sim 509$  nm for 7 layer/ATO. Each coated sol-layer has a thickness of  $\sim 25$ – $35$  nm on the ATO thin films. In addition, the cross-sectional FESEM image (f) of the 0 layer/ATO thin film shows a more porous structure compared to those of the other samples coated with sol-layers (g–j).

Fig. 4 shows AFM images of the 0 layer/ATO and 5 layer/ATO thin films, which allow us to further examine the surface morphology of the samples. The surface morphological properties of thin films directly affect the electrical properties. Obtaining a dense surface on the thin films is a key goal for improving the performance of TCOs. The average surface roughness is  $\sim 9.95$  nm for the 0 layer/ATO and  $\sim 5.66$  nm for the 5 layer/ATO thin film. These results imply that the 5 layer/ATO thin film has a dense surface morphology compared to the 0 layer/ATO thin film because the ATO sol-solution, which consists of Sn and Sb precursors dissolved in 2-propanol, fills the gaps between grains in ATO thin films with porous structures. This decreases the inter-grain boundary size, resulting in improved electrical performance of the TCOs. Thus, the AFM results are in good agreement with the FESEM images.

Fig. 5 shows TEM and high-resolution TEM images of the ATO nanoparticles obtained after hydrothermal treatment, ATO nanoparticles obtained after the 0 layer/ATO thin film using spin-coating, and ATO nanoparticles obtained after the 5 layer/ATO thin film using spin-coating. For the TEM measurements, all the

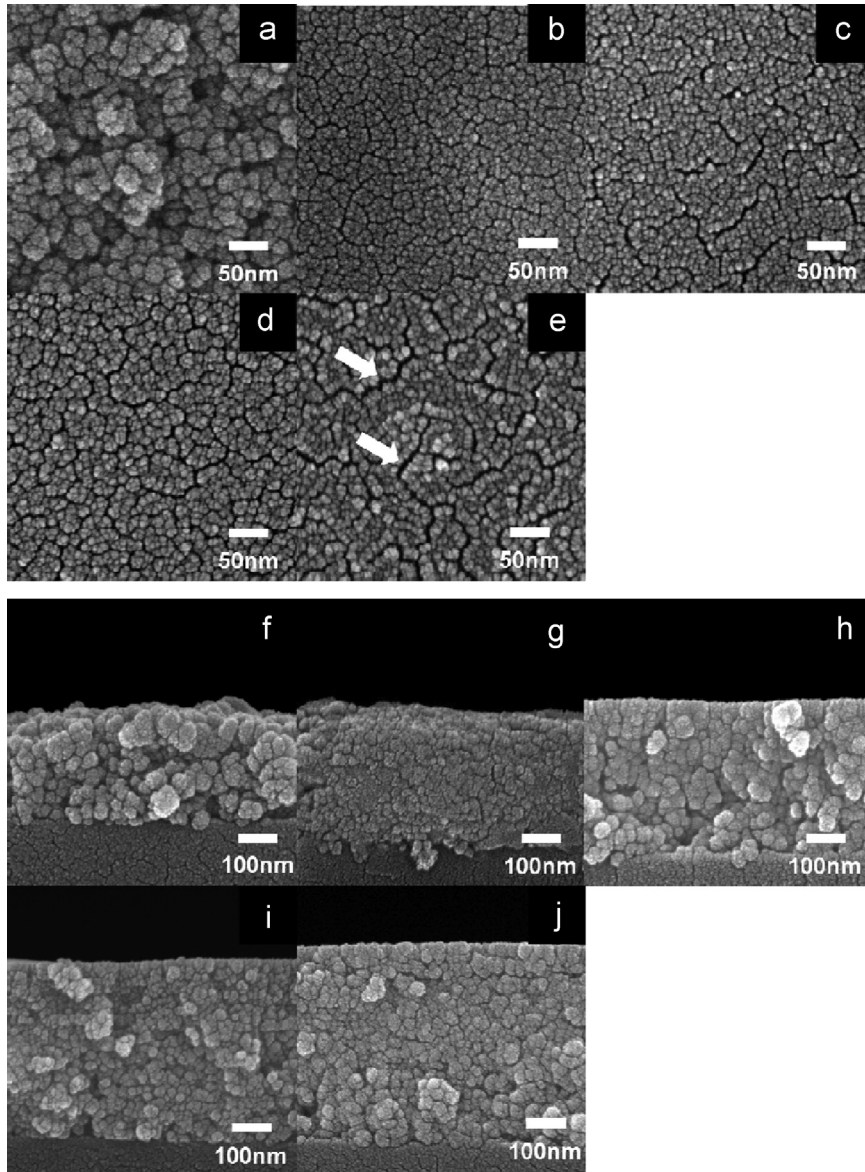


Fig. 3. Top-view FESEM images (a–e) and cross-section FESEM images (f–j) of the 0 layer/ATO, 1 layer/ATO, 3 layer/ATO, 5 layer/ATO, and 7 layer/ATO thin films.

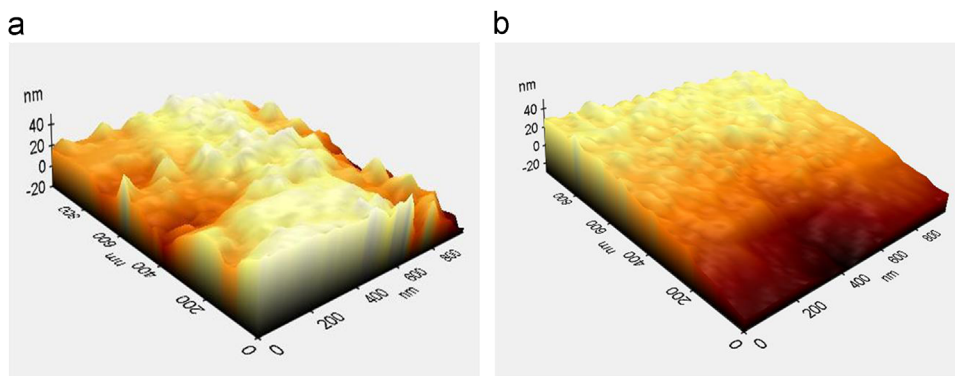


Fig. 4. AFM images of the 0 layer/ATO and 5 layer/ATO thin films.

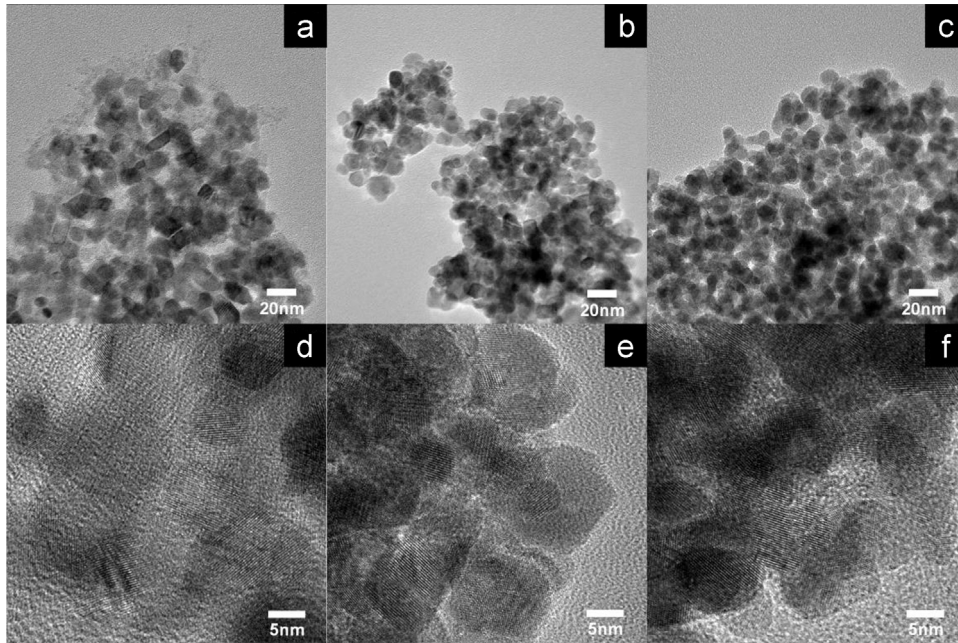


Fig. 5. TEM and high-resolution TEM images of the ATO nanoparticles obtained after hydrothermal treatment (a, d), ATO nanoparticles obtained after the 0 layer/ATO thin film using spin-coating (b, e), and ATO nanoparticles obtained after the 5 layer/ATO thin films using spin-coating (c, f).

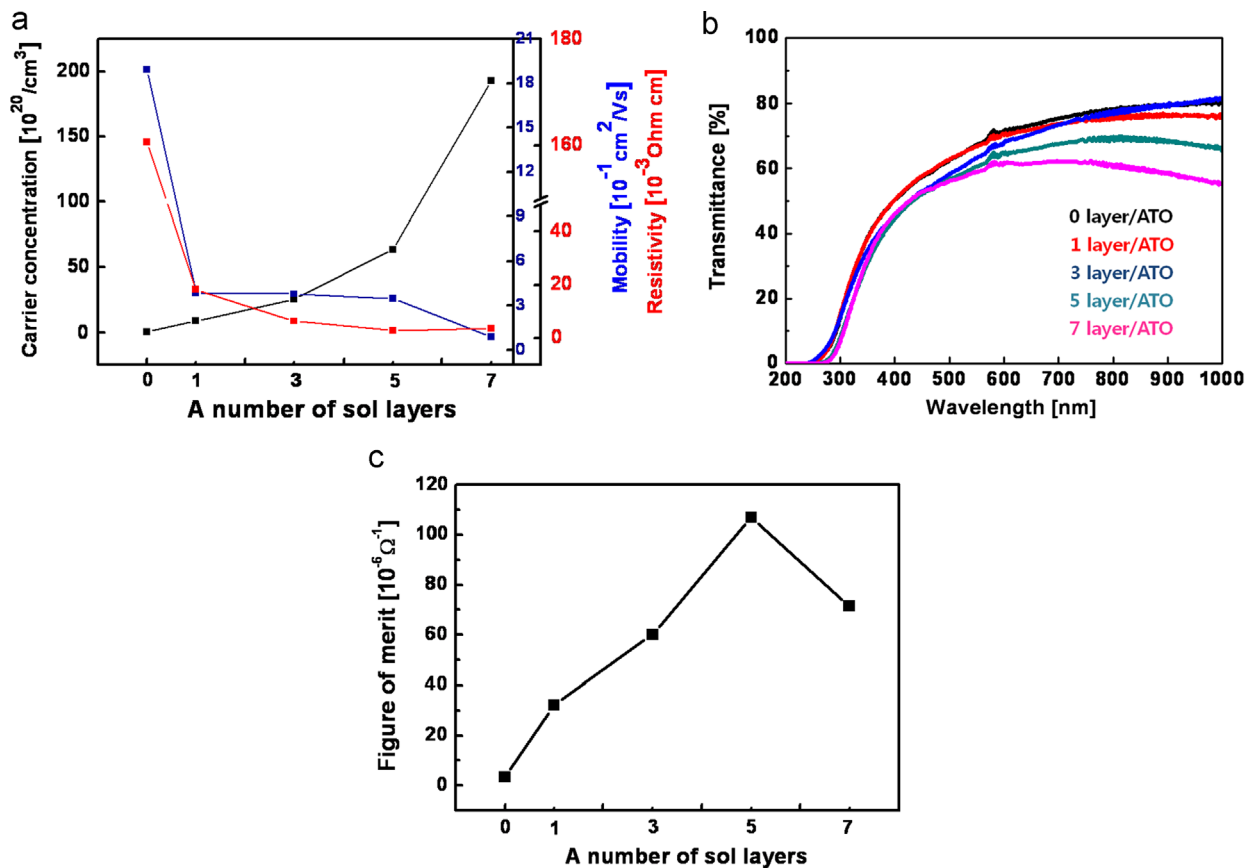


Fig. 6. The electrical properties including the carrier concentration, Hall mobility, and resistivity (a), the optical transmission spectra (b), and the figure of merit obtained from all the samples (c).

samples are dispersed in ethanol using ultrasonication for 0.5 h. Then, the samples are placed on a TEM grid. The average particle sizes are in the ranges of ~6.6–20.8 nm for the ATO nanoparticles

after hydrothermal treatment, ~5.5–18.2 nm for the 0 layer/ATO thin films, and ~6.8–16.9 nm for the 5 layer/ATO thin films. All the samples also have similar nanoparticle sizes and distributions.

Table 1

Summary of electrical and optical properties for the 0 layer/ATO, 1 layer/ATO, 3 layer/ATO, 5 layer/ATO, and 7 layer/ATO thin films.

Sample	Carrier concentration (cm <sup>-3</sup> )	Hall mobility (cm <sup>2</sup> /Vs)	Resistivity (Ω cm)	Sheet resistance (Ω/square)	Transmittance (%)
0 layer/ATO	2.74 × 10 <sup>19</sup>	1.892	1.60 × 10 <sup>-1</sup>	5.5 × 10 <sup>3</sup>	67.26
1 layer/ATO	8.85 × 10 <sup>20</sup>	3.86 × 10 <sup>-1</sup>	1.82 × 10 <sup>-2</sup>	562.15	66.94
3 layer/ATO	2.54 × 10 <sup>21</sup>	3.80 × 10 <sup>-1</sup>	6.44 × 10 <sup>-3</sup>	169.26	63.20
5 layer/ATO	6.37 × 10 <sup>21</sup>	3.47 × 10 <sup>-1</sup>	2.81 × 10 <sup>-3</sup>	62.02	60.55
7 layer/ATO	1.93 × 10 <sup>22</sup>	8.98 × 10 <sup>-2</sup>	3.59 × 10 <sup>-3</sup>	69.92	58.86

In addition, as shown in Fig. 5(d–f), the ATO nanoparticles obtained after a hydrothermal method at 240 °C show amorphous and crystalline characteristics. However, for the 0 layer/ATO and 5 layer/ATO thin films, the ATO nanoparticles obtained after microwave irradiation at 550 °C show superior crystallinity, leading to the high-performance of the TCOs.

Fig. 6(a) shows the carrier concentration, Hall mobility, and resistivity of all the samples. The carrier concentration increases gradually with increasing film thickness. That is, the carrier concentration improves from 2.74 × 10<sup>19</sup> cm<sup>-3</sup> for 0 layer/ATO to 1.93 × 10<sup>22</sup> cm<sup>-3</sup> for 7 layer/ATO. As for the Hall mobility, 0 layer/ATO thin film exhibits a high mobility of 1.89 cm<sup>2</sup>/Vs because of its lower carrier concentration of 2.74 × 10<sup>19</sup> cm<sup>-3</sup> relative to the other samples. In addition, the 1 layer/ATO, 3 layer/ATO, and 5 layer/ATO thin films have similar low mobilities: 3.86 × 10<sup>-1</sup>, 3.80 × 10<sup>-1</sup>, and 3.47 × 10<sup>-1</sup> cm<sup>2</sup>/Vs due to small sizes of ATO nanoparticles. However, the 7 layer/ATO thin film has the lowest mobility, 8.98 × 10<sup>-2</sup> cm<sup>2</sup>/Vs, because of the formation of cracks, as shown in Fig. 3(e). Therefore, the resistivity ( $\rho$ ) of the thin films can be explained by the following equation including the carrier concentration and Hall mobility [3]:

$$\rho = 1/(Ne\mu)$$

where  $N$  is the carrier concentration,  $\mu$  is the Hall mobility, and  $e$  is the electron charge (1.602 × 10<sup>-19</sup> C). That is, the resistivity ( $\rho$ ) of the thin films is in inverse proportion to the carrier concentration ( $N$ ) and Hall mobility ( $\mu$ ). Thus, the values of the resistivity ( $\rho$ ) are ~1.60 × 10<sup>-1</sup> Ω cm for 0 layer/ATO, ~1.82 × 10<sup>-2</sup> Ω cm for 1 layer/ATO, ~6.44 × 10<sup>-3</sup> Ω cm for 3 layer/ATO, ~2.81 × 10<sup>-3</sup> Ω cm for 5 layer/ATO, and ~3.59 × 10<sup>-3</sup> Ω cm for 7 layer/ATO. The sheet resistance can also be calculated considering the resistivity/thickness, as ~5.5 × 10<sup>3</sup> Ω/□ for 0 layer/ATO, ~562.15 Ω/□ for 1 layer/ATO, ~169.26 Ω/□ for 3 layer/ATO, ~62.02 Ω/□ for 5 layer/ATO, and ~69.92 Ω/□ for 7 layer/ATO. Therefore, 5 layer/ATO thin films exhibit superb electrical properties compared to the other samples, which can be explained by two reasons: one is densification and thickness increase of the thin films due to the introduction of optimum sol-layers. The other is the dominant increase of the carrier concentration with small decrease of the electron mobility. Fig. 6(b) shows optical transmission spectra of all the samples. The transmittances at 550 nm are ~67.26% for 0 layer/ATO, ~66.94% for 1 layer/ATO, ~63.20% for 3 layer/ATO, ~60.55% for 5 layer/ATO, and ~58.86% for 7 layer/ATO. Thus, the transmittance of the

samples decreases with increasing thickness of the thin films. The results including the electrical and optical properties are summarized in Table 1. Fig. 6(c) shows the figure of merit (FOM) for all the samples for evaluation of the performance. The FOM can be calculated using the following equation [19]:

$$\text{FOM} = T^{10}/R_s$$

where  $T$  is the transmittance of the films and  $R_s$  is the sheet resistance. Thus, the values of FOM are observed to be 3.45 × 10<sup>-6</sup> Ω<sup>-1</sup> for 0 layer/ATO, 3.21 × 10<sup>-5</sup> Ω<sup>-1</sup> for 1 layer/ATO, 6.01 × 10<sup>-5</sup> Ω<sup>-1</sup> for 3 layer/ATO, 1.07 × 10<sup>-4</sup> Ω<sup>-1</sup> for 5 layer/ATO, and 7.14 × 10<sup>-5</sup> Ω<sup>-1</sup> for 7 layer/ATO. That is, the 5 layer/ATO thin film has a superb FOM among these samples. These results imply that ATO thin films coated with 5 sol-layers have excellent resistivity, good transmittance, and an excellent FOM among solution-based TCOs.

#### 4. Conclusions

Solution-based TCOs with ATO thin films were fabricated using a hydrothermal method and spin-coating. Their structures, chemical states, surface morphology, and electrical and optical properties were characterized by XRD, XPS, FESEM, AFM, TEM, Hall effect measurement, and UV–vis spectrophotometry. To investigate the effect of the sol-layer, we formed to be 0, 1, 3, 5, and 7 sol-layers on ATO thin films with porous structures. The sol-layer coated on ATO thin films can lead to the formation of a dense surface morphology due to the decreased inter-grain boundary size and the increase of thickness. In particular, ATO thin films coated with 5 sol-layers exhibited superb resistivity (~2.81 × 10<sup>-3</sup> Ω cm), good transmittance (~60.55%), and a superb FOM (~1.3 × 10<sup>-4</sup> Ω<sup>-1</sup>). Solution-based ATO thin films coated with the optimum number of sol-layers may be promising candidates in potential TCO applications.

#### Acknowledgment

This work was supported by Grant no. 10041161 from the Ministry of Knowledge Economy (MKE) and Fundamental R&D Program for Core Technology of Materials funded by the Ministry of Knowledge Economy, Republic of Korea.

## References

- [1] S.H. Park, J.B. Park, P.K. Song, Characteristics of Al-doped, Ga-doped and In-doped zinc-oxide films as transparent conducting electrodes in organic light-emitting diodes, *Current Applied Physics* 10 (2010) S488–S490.
- [2] D. Slocombe, A. Porch, M. Pepper, P.P. Edwards, The mott transition and optimal performance of transparent conducting oxides in thin-film solar cells, *Energy and Environmental Science* 5 (2012) 5387.
- [3] S. Calnan, A.N. Tiwari, High mobility transparent conducting oxides for thin film solar cells, *Thin Solid Films* 518 (2010) 1839–1849.
- [4] C. Guillen, J. Herrero, TCO/metal/TCO structures for energy and flexible electronics, *Thin Solid Films* 520 (2011) 1–17.
- [5] U. Betz, M.K. Olsson, J. Marthy, M.F. Escola, F. Atammy, Thin films engineering of indium tin oxide: large area flat panel displays application, *Surface and Coatings Technology* 200 (2006) 5751–5759.
- [6] T.R. Giraldi, M.T. Escote, M.I.B. Bernardi, V. Bouquet, E.R. Leite, E. Longo, J.A. Varela, Effect of thickness on the electrical and optical properties of Sb doped SnO<sub>2</sub> (ATO) thin films, *Journal of Electroceramics* 13 (2004) 159–165.
- [7] X. Hao, J. Ma, D. Zhang, X. Xu, Y. Yang, H. Ma, S. Ai, Transparent conducting antimony-doped tin oxide films deposited on flexible substrates by r.f. magnetron-sputtering, *Applied Physics A* 75 (2002) 397–399.
- [8] J. Kane, H.P. Schweizer, W. Kern, Chemical vapor deposition of antimony-doped tin oxide films formed from dibutyl tin diacetate, *Journal of the Electrochemical Society* 123 (1976) 270–277.
- [9] K.S. Shamala, L.C.S. Murthy, K.N. Rao, Studies on tin oxide films prepared by electron beam evaporation and spray pyrolysis methods, *Bulletin of Material Science* 27 (2004) 295–301.
- [10] R.M. Pasquarelli, D.S. Ginley, R. O'Hayre, Solution processing of transparent conductor: from flask to film, *Chemical Society Reviews* 40 (2011) 5406–5441.
- [11] D. Burgard, C. Goebbert, R. Nass, Synthesis of nanocrystalline, redispersible antimony-doped SnO<sub>2</sub> particles for the preparation of conductive, transparent coatings, *Journal of Sol–Gel Science and Technology* 13 (1998) 789–792.
- [12] M.S. Hwang, B.Y. Jeong, J.H. Moon, S.K. Chun, J.H. Kim, Inkjet-printing of indium tin oxide (ITO) films for transparent conducting electrodes, *Materials Science and Engineering B* 176 (2011) 1128–1131.
- [13] J.S. Fang, W.H. Luo, S.H. Hsu, J.C. Yang, T.K. Tsai, The transparent conductive properties of manganese-doped zinc oxide films deposited by chemical bath deposition, *Journal of Electronic Materials* 41 (2012) 122–129.
- [14] J. Zhang, L. Gao, Synthesis and characterization of antimony-doped tin oxide (ATO) nanoparticles, *Inorganic Chemistry Communications* 7 (2004) 91–93.
- [15] M. Oztas, M. Bedir, Thickness dependence of structural, electrical and optical properties of sprayed ZnO:Cu films, *Thin Solid Films* 516 (2008) 1703–1709.
- [16] Y.G. Her, J.Y. Wu, Y.R. Lin, S.Y. Tsai, Low-temperature growth and blue luminescence of SnO<sub>2</sub> nanoblades, *Applied Physics Letters* 89 (2006) 043115.
- [17] C. Goebbert, H. Bisht, N. Al-Dahoudi, R. Nonninger, M.A. Aegerter, H. Schmidt, Wet chemical deposition of crystalline, redispersible ATO and ITO nanoparticles, *Journal of Sol–Gel Science and Technology* 19 (2000) 201–204.
- [18] J.P. Chatelon, C. Terrier, E. Bernstein, R. Berjoan, J.A. Roger, Morphology of SnO<sub>2</sub> thin films obtained by the sol–gel technique, *Thin Solid Films* 247 (1994) 162–168.
- [19] J. Liu, A.W. Hains, J.D. Servaites, M.A. Ratner, T.J. Marks, Highly conductive bilayer transparent conducting oxide thin films for large-area organic photovoltaic cells, *Chemistry of Materials* 21 (2009) 5258–5263.